 CMC, vol.16, no.1, pp.25-49, 2010

# Invariant Based Transversely-Isotropic Material and Failure Model for Fiber-Reinforced Polymers

**M. Vogler[1], G. Ernst[1] and R. Rolfes[1]**

**Abstract:** In this article, a constitutive formulation of a transversely-isotropic material and failure model for fiber-reinforced polymers is presented comprising pre-failure material nonlinearities, a novel invariant based quadratic failure criterion (IQC) as well as post failure material softening. The failure surface of the IQ criterion is assumed to take the influence of triaxiality on fracture into account. Further, a distinction between fiber failure and inter-fiber failure is conducted. Material softening is governed by a fracture energy formulation and the introduction of an internal length. The constitutive model is implemented into a programming user interface of the commercial finite element program Abaqus. As results, different laminate lay-ups are modelled and exposed to different stress states in an FE analysis. The obtained failure surfaces and stress strain curves for each laminate lay-up are compared to experimental data. As further applications of the material model presented, a curved composite beam, showing delamination, and a 0°/90°/0°-rod, showing the characteristic damage state in the 90°layer, are simulated and compared to tests.

**Keywords:** transverse isotropy, shear nonlinearities, failure, fracture energy.

## 1 Introduction

Due to their great potential for weight savings, fiber reinforced polymer laminates are becoming increasingly important for light weight design in aerospace, wind energy, mechanical and civil engineering. In order to exploit the advantages of fiber reinforced polymer laminates (FRP laminates), reliable prediction of the mechanical behavior, particularly the onset and propagation of failure of such laminates, is essential. A variety of failure criteria has been developed and published in literature. [Nahas (1986)] gives a review of about 30 criteria. A very important selection of leading failure and post failure theories is included in the World-Wide-Failure-Exercise (WWFE), conceived and conducted by [Hinton, Kaddour,

[1] ISD, Leibniz Universität Hannover, Germany.

and Soden (2004)]. The WWFE is the result of a project known as the "Failure Olympics", in which contributors around the world tested the accuracy of various theories for predicting deformation and failure strength of laminated composite structures. Within the exercise, the leading failure theories for composite laminates are described by their originators and used by them to solve a prescribed set of problems. The criterion of [Tsai and Wu (1971)] was published among the first and is probably the most often used criterion. It employs a single global, quadratic failure condition and thus is very efficient in computational cost. Due to the single global formulation, it does not provide information about the type of failure, which is, however, very important for the design engineer in order to judge about the criticality of failure. The substantial differentiation between fiber-failure and inter-fiber failure was first postulated by [Puck and Schneider (1969)]. It was taken up by [Hashin (1980)] and enhanced by use of invariants and a Mohr-coulomb fracture approach. The latter was considered as computationally costly at that time, therefore it was no longer pursued until it was taken up again by [Puck (1996)]. Criteria that differentiate failure modes, e.g. [Puck and Schürmann (2004); Cuntze and Freund (2004)], have proven their reliability in the WWFE. A further outcome of the WWFE is, that pre-failure material nonlinearities and post-failure material softening are as well very important for a realistic failure description.

In general, damage in fiber reinforced polymers can be modeled at different levels, at sub-ply level and at ply level. Sub-ply level damage models are able to regard different failure mechanisms, that occur in a single ply of a laminate, such as matrix cracking, delamination and fiber failure. Delamination is normally simulated using methods based on linear-elastic fracture mechanics, such as the virtual crack closure technique [Krueger, Paris, O'Brien, and Minguet (2002)], or using cohesive formulations [Allix and Corigliano (1999); Turon, Camanho, Costa, and Dávila (2006); Turon, Camanho, Costa, and Renart (2010); Camanho, Dávila, and Moura (2003)]. [Pinho, Dávila, Ianucci, and Robinson (2004)] developed a fully three-dimensional continuum damage model at sub-ply level able to predict both the intralaminar and the interlaminar failure mechanisms of fiber-reinforced polymer composites in an integrated way. Thus it is possible to model the effects of transverse matrix cracks on the residual stiffness of laminates, the interaction between transverse matrix cracks and delamination, and final failure of the laminate. Another approach, regarding both delamination and ply failure is to combine cohesive elements that simulate delamination with continuum damage models that simulate ply damage [Hallett, Green, Jiang, and Wisnom (2009)].

Ply level continuum damage models are a computationally very efficient way of modeling damage in fiber reinforced composites. In contrast to sub-ply level damage models, these kind of damage models consider the actual discontinuous material of a ply embedded in a laminate as a homogenized material showing the same

effective material behavior. The damage variables are derived as thermodynamic conjugate variables from the Helmholtz free energy. Some of the most prominent ones are those developed at LMT Cachan, see [Ladevèze, Allix, Deü, and Lèvêque (2000); Allix, Feissel, and Thévenet (2003)], which have been adopted by several other authors. Further models can be found in [Barbero and Cortes (2010); Schuecker and Pettermann (2006)]. Recent developments in this field are the works of [Maimí, Mayugo, and Camanho (2008); Maimí, Camanho, Mayugo, and Dávila (2007a); Maimí, Camanho, Mayugo, and Dávila (2007b)].
In the following, a novel nonlinear material model and a stress based quadratic failure criterion are presented, modelling the lamina material behavior on sub-ply level. The constitutive equations and the invariant based failure criterion are explained in detail. Finally, numerical results are shown and compared to experimental data. At first, laminates presented in the WWFE are modeled and compared to test data. Experimentally determined failure envelopes in stress space as well as pre- and post failure behavior of the tested laminates are predicted in the simulations. As a further example, a progressive failure analysis is performed at an FE model of a curved composite beam, where the onset and growth of delamination caused by out of plane normal tensile stresses is investigated. Finally, the characteristic damage state in a (0°/90°/0°)-rod is simulated and prediction of the experimentally confirmed remaining stiffness (in-situ effect). A further application of this material model is the modelling of single plies of textile composites within the framework of a multiscale analysis for determination of stiffnesses and strengthes of textile non-crimped fabrics. This approach is explained in detail in [Ernst (2009); Ernst, Vogler, Hühne, and Rolfes (2010)].

## 2 Constitutive Model

UD-composites exhibit a strong direction dependent mechanical behavior, which can be assumed as transversely-isotropic. The mechanical behavior can be traced back to the properties of the constituents, fiber and matrix. The mode of loading determines the properties, which finally prevail. In fiber direction the characteristics of the fiber take effect, whereas in transverse direction the characteristics of the matrix predominate. Accordingly, the behavior in fiber direction is linear elastic until fracture, whereas under longitudinal and transverse shear stress states as well as under transverse compression, pronounced nonlinearities are observed. In order to find an adequate modelling approach, it is very important to capture these different behavior. The observed nonlinearities, see Fig. 1, are caused by plastic deformations of the matrix as well as by damage and viscous effects. From an experimental point of view it is a challenging task to distinguish between these different effects. In the material model presented, the focus is laid on capturing the nonlinear mate-

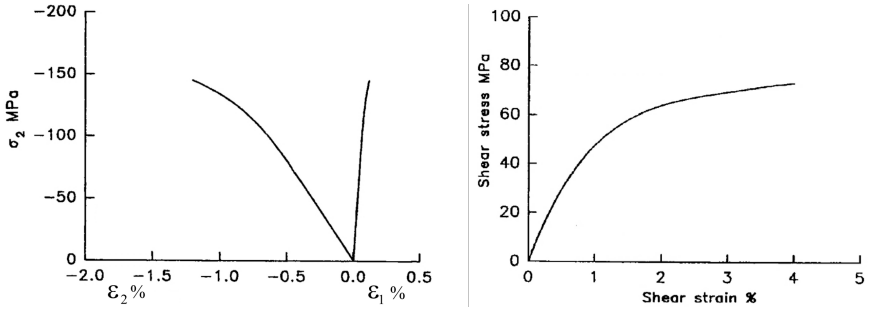


(a) Transverse compressive loading (b) In-plane shear loading

Figure 1: Nonlinear material behavior of an E-glass/epoxy lamina, taken from [Hinton, Kaddour, and Soden (2004)]

rial behavior by neglecting the causation. Hence, as a simplified assumption, the observed nonlinearities are considered to be plastic and an elastic plastic material law is chosen to model these nonlinearities.

The constitutive equations are developed by means of structural tensors in the framework of invariant theory. In contrast to conventional methods describing anisotropy by using symmetry conditions, this approach alleviates the derivation of the constitutive equations as well as the determination of material parameters significantly. Furthermore a coordinate system independent representation of the constitutive equations is obtained. Transversely-isotropic materials are characterized by a preferred direction **a**. Thus, the material response is invariant with respect to arbitrary rotations around this preferred direction **a**, to reflections at fiber parallel planes and with respect to the reflection at that plane, whose normal is **a**. These are the group of symmetry transformations for transverse isotropy. The structural tensor **A** of transverse isotropy, which represents the material's intrinsic characteristic, is defined as the dyadic product of the preferred direction **a**

$$\mathbf{A} = \mathbf{a} \otimes \mathbf{a} \quad . \tag{1}$$

As the elastic range of the material is assumed to be small, an additive decomposition of the strain tensor is justified:

$$\varepsilon = \varepsilon^e + \varepsilon^p \quad . \tag{2}$$

In the subsequent representations, isotropic tensor functions for the elastic free energy and the yield surface are derived.

### *2.1 Elastic Stress Strain Relations*

Considering only small elastic deformations, HOOKE's linear elasticity law $\sigma = \hat{\sigma}(\varepsilon) = \mathbb{C}_e \varepsilon$ is assumed. Postulating hyperelasticity, the first derivative of the free energy function $\hat{\Psi}$ with respect to the strains $\varepsilon$ yields the stresses $\sigma$ and the second derivation with respect to the strains $\varepsilon$ gives the elasticity tensor $\mathbb{C}_e$. In case of transverse isotropy, the free energy function is formulated in isotropic invariants of the strain tensor $\varepsilon$ and the structural tensor $\mathbf{A}$, see [Boehler (1987)]. To derive a representation of $\hat{\Psi}$ and the infinitesimal stress tensor $\sigma$ as isotropic tensor-functions, the functional basis of the two symmetric second order tensorial arguments $\sigma$ and $\mathbf{A}$ is needed. Assuming the stresses to be a linear function of the strains and providing a stress free undistorted initial configuration, i.e. $\sigma(\varepsilon = 0) = 0$, such terms are neglected, which are linear or cubic in the strains. This enforces the elasticity tensor $\mathbb{C}_e$ to be constant and yields to a formulation of the free energy function with five elasticity constants $\lambda$, $\alpha$, $\mu_L$, $\mu_T$ and $\beta$ describing the transversely-isotropic material behavior:

$$\begin{aligned} \hat{\Psi}(\varepsilon, \mathbf{A}) := \quad & \frac{1}{2}\lambda(\operatorname{tr}\varepsilon)^2 + \mu_T \operatorname{tr}(\varepsilon)^2 + \alpha(\mathbf{a}\varepsilon\mathbf{a}) \operatorname{tr}\varepsilon + \\ & 2(\mu_L - \mu_T)(\mathbf{a}\varepsilon^2\mathbf{a}) + \frac{1}{2}\beta(\mathbf{a}\varepsilon\mathbf{a})^2 \quad . \end{aligned} \tag{3}$$

For the stresses one obtains

$$\begin{aligned} \sigma = \quad & \lambda(\operatorname{tr}\varepsilon)\mathbf{1} + 2\mu_T\varepsilon + \alpha(\mathbf{a}\varepsilon\mathbf{a}\,\mathbf{1} + \operatorname{tr}\varepsilon\,\mathbf{A}) \\ & + 2(\mu_L - \mu_T)(\mathbf{A}\varepsilon + \varepsilon\mathbf{A}) + \beta\,(\mathbf{a}\varepsilon\mathbf{a})\,\mathbf{A} \end{aligned} \tag{4}$$

and the elasticity tensor is written as

$$\begin{aligned} \mathbb{C}_e = \quad & \lambda\mathbf{1}\otimes\mathbf{1} + 2\mu_T\mathbb{I} + \alpha(\mathbf{A}\otimes\mathbf{1} + \mathbf{1}\otimes\mathbf{A}) \\ & + 2(\mu_L - \mu_T)\mathbb{I}_{\mathbf{A}} + \beta\mathbf{A}\otimes\mathbf{A} \quad , \end{aligned} \tag{5}$$

where

$$\mathbb{I}_{\mathbf{A}} = A_{im}\mathbb{I}_{jmkl} + A_{jm}\mathbb{I}_{mikl} \quad . \tag{6}$$

In matrix notation the 4th order elasticity tensor of transversely-isotropic material for a preferred $X_1$-direction in a Cartesian coordinate system, i.e. $\mathbf{a} = [1,0,0]$, reads:

$$\mathbb{C}_e = \begin{bmatrix} \lambda + 2\alpha + \beta + 4\mu_L - 2\mu_T & \lambda + \alpha & \lambda + \alpha & 0 & 0 & 0 \\ \lambda + \alpha & \lambda + 2\mu_T & \lambda & 0 & 0 & 0 \\ \lambda + \alpha & \lambda & \lambda + 2\mu_T & 0 & 0 & 0 \\ 0 & 0 & 0 & \mu_L & 0 & 0 \\ 0 & 0 & 0 & 0 & \mu_L & 0 \\ 0 & 0 & 0 & 0 & 0 & \mu_T \end{bmatrix} \quad . \tag{7}$$

### 2.2 Transversely-isotropic Yield Surface

This proposal of a transversely-isotropic yield surface is an extension of a yield function following [Rogers (1987); Spencer (1987)] and its numerical treatment in [Schröder (1995); Eidel (2004)]. This model is based on two assumptions, on plastic incompressibility and that projections of stresses onto the preferred direction $\mathbf{a}$ do not induce plastic yielding. This condition is taken into account by a decomposition of the stress tensor into an extra stress tensor $\sigma^{\text{pind}}$, inducing plastic yielding, and a remaining reaction stress tensor $\sigma^{\text{reac}}$:

$$\sigma = \sigma^{\text{pind}} + \sigma^{\text{reac}} \quad . \tag{8}$$

The assumption of plastic incompressibility is fulfilled with the postulation

$$\operatorname{tr}\sigma^{\text{pind}} = 0 \quad . \tag{9}$$

Presuming inextensibility of the preferred direction $\mathbf{a}$, in which plasticity is assumed not to occur, leads to an additional constraint. The projection of the stress tensor onto the fiber direction $\mathbf{a}$ must vanish:

$$\mathbf{a}\sigma^{\text{pind}}\mathbf{a} = \mathbf{a}\otimes\mathbf{a} : \sigma^{\text{pind}} = 0 \quad . \tag{10}$$

$\mathbf{A}$ is the structural tensor belonging to the fiber direction $\mathbf{a}$. With Eq. (9), Eq. (10) and an ansatz for $\sigma^{\text{reac}}$ of the form

$$\sigma^{\text{reac}} = p\mathbf{1} + T_a\mathbf{A} \quad , \tag{11}$$

the stress components $\sigma^{\text{reac}}$ and $\sigma^{\text{pind}}$ yield

$$\begin{aligned} \sigma^{\text{reac}} &= \frac{1}{2}(\operatorname{tr}\sigma - \mathbf{a}\sigma\mathbf{a})\mathbf{1} - \frac{1}{2}(\operatorname{tr}\sigma - 3\mathbf{a}\sigma\mathbf{a})\mathbf{A} \\ \sigma^{\text{pind}} &= \sigma - \frac{1}{2}(\operatorname{tr}\sigma - \mathbf{a}\sigma\mathbf{a})\mathbf{1} + \frac{1}{2}(\operatorname{tr}\sigma - 3\mathbf{a}\sigma\mathbf{a})\mathbf{A} \quad . \end{aligned} \tag{12}$$

As can be seen in the following equation, $T_a$ can be interpreted as a fiber overstress, exceeding the hydrostatical part of the stress tensor. The total stress of the fiber is

$$\mathbf{a}\sigma\mathbf{a} = \mathbf{a}\sigma^{\text{reac}}\mathbf{a} = p + T_a \quad . \tag{13}$$

To account for an influence of plastification in fiber direction, the projection of the deviatoric part of the reaction stress tensor $\sigma^{\text{reac}}$ onto $\mathbf{a}$ can be regarded:

$$\mathbf{a}(\operatorname{dev}\sigma^{\text{reac}})\mathbf{a} = \mathbf{a}\,T_a(\operatorname{dev}\mathbf{A})\mathbf{a} = T_a\,\mathbf{a}(\mathbf{A} - \frac{1}{3}\mathbf{1})\mathbf{a} = \frac{2}{3}T_a \quad . \tag{14}$$

The construction of the anisotropic yield condition follows the same considerations as the derivation of the hyperelastic potential $\hat{\Psi}$. The yield function has to be invariant with respect to transformations belonging to the group of symmetry transformations for transverse isotropy. The yield condition can be composed of the basic invariants of the related stresses and the structural tensor. The invariants $I_1$ and $I_2$ are formulated with $\sigma^{\text{pind}}$, following a proposal of [Schröder (1995)], who refers to the work of [Spencer (1987); Rogers (1987)]:

$$\begin{aligned} I_1 &:= \frac{1}{2}\,\mathrm{tr}\,(\sigma^{\text{pind}})^2 - \mathbf{a}\,(\sigma^{\text{pind}})^2\,\mathbf{a} \quad , \\ I_2 &:= \mathbf{a}\,(\sigma^{\text{pind}})^2\,\mathbf{a} \quad . \end{aligned} \tag{15}$$

If only these two invariants are considered in the yield locus, solely shear deformations are assumed to cause plastic yielding. If yielding in the preferred fiber direction should be considered, an additional invariant, formulated in deviatoric stresses, is introduced:

$$I_4 := \frac{3}{2}\mathbf{a}\sigma^{\text{dev}}\mathbf{a} = T_a \quad . \tag{16}$$

In order to account for a pressure dependency of the yield locus, a further invariant, representing the hydrostatical pressure is introduced:

$$I_3 := \mathrm{tr}\,\sigma - \mathbf{a}\sigma\mathbf{a} \quad . \tag{17}$$

The yield function as a function of the introduced invariants is formulated as

$$f = \alpha_1 I_1 + \alpha_2 I_2 + \alpha_3 I_3 + \alpha_{32} I_3^2 + \alpha_4 I_4^2 - 1 \tag{18}$$

with the flow parameters $\alpha_1$, $\alpha_2$, $\alpha_3$, $\alpha_{32}$ and $\alpha_4$. The derivations of the yield surface are:

$$\begin{aligned} \partial_\sigma f &= \partial_{I_i} f\,\partial_\sigma I_i = \\ &\quad \alpha_1\,\sigma^{\text{pind}} + (\alpha_2 - \alpha_1)\,(\mathbf{A}\,\sigma^{\text{pind}} + \sigma^{\text{pind}}\mathbf{A}) + \alpha_3(\mathbf{1} - \mathbf{A}) \\ &\quad + 2\alpha_{32} I_3(\mathbf{1} - \mathbf{A})\alpha_4\,(3\,I_4\mathbf{A}^{\text{dev}}) \;=:\; \mathbb{A} : \sigma + \mathbf{B} \\ \partial^2_{\sigma\sigma} f &= \alpha_1\,\mathbb{P}^{\text{pind}} + (\alpha_2 - \alpha_1)\,\mathbb{P}^{\text{pind}}_{\mathbf{A}} + 2\alpha_{32}(\mathbf{1} - \mathbf{A}) \otimes (\mathbf{1} - \mathbf{A}) \\ &\quad + \alpha_3(\mathbf{1} - \mathbf{A})\frac{9}{2}\,\alpha_4\,\mathbf{A}^{\text{dev}} \otimes \mathbf{A}^{\text{dev}} \;=:\; \mathbb{A} \end{aligned} \tag{19}$$

with the projection tensors

$$\begin{aligned} \mathbb{P}^{\text{pind}} &:= \partial_\sigma \sigma^{\text{pind}} = \mathbb{I} - \tfrac{1}{2}(\mathbf{1} \otimes \mathbf{1}) + \tfrac{1}{2}(\mathbf{A} \otimes \mathbf{1} + \mathbf{1} \otimes \mathbf{A}) - \frac{3}{2}(\mathbf{A} \otimes \mathbf{A}) \\ (\mathbb{P}^{\text{pind}}_{\mathbf{A}})_{ijkl} &:= A_{im}\mathbb{P}^{\text{pind}}_{mjkl} + A_{mj}\mathbb{P}^{\text{pind}}_{imkl} \quad . \end{aligned} \tag{20}$$

$\mathbf{A}^{\text{dev}}$ is the deviator of the structural tensor $\mathbf{A}$, $\mathbb{A}$ is the constant bending tensor and $\mathbf{B}$ is the first derivative of the linear terms in $\sigma$ of the quadratic yield locus. This enables us to state the yield function Eq. (18) in the more general form

$$f = \frac{1}{2}\sigma : \mathbb{A} : \sigma + \mathbf{B} : \sigma - 1 \quad . \tag{21}$$

### *2.3 Hardening Formulation*

In the material law presented, an isotropic hardening model is implemented. The hardening formulation is fully tabulated and consequently, the user can directly input measurement results from material testings in terms of load curves giving the yield stress as a function of the corresponding plastic strain. Thus, test results that are reflected in the load curves will be used exactly in the simulation without time consuming parameter fitting. The tabulated input of hardening curves requires true stresses over true plastic strains. As the hardening curves usually are measured as stresses over total strains, the curves have to be prepared by subtracting the elastic part of the strains from the total strains. If hardening data are given as engineering stresses and engineering strains, a conversion into true stresses and true strains has to be performed.

#### *2.3.1 Parameter Identification*

In order to determine the five material parameters $\alpha_1$, $\alpha_2$, $\alpha_3$, $\alpha_{32}$ and $\alpha_4$ of the yield function Eq. (18), five material tests are required, giving the yield stresses over the plastic strains. Concerning the numerical treatment, a table lookup is performed in every time step and the yield surface parameters are updated. As input serve the corresponding plastic strain for each material test. In the sequel, the conversion of the yield stresses $y$ into the yield surface parameters are derived. The chosen material tests should be understood as an example of a possible set of tests. Of course, any of these testings can be replaced by other suitable material tests if available. The following five material tests are suggested to determine the yield surface parameters :

1. tension in fiber direction

$$\sigma = \operatorname{dev}\sigma = \begin{bmatrix} y_a & 0 & 0 \\ 0 & 0 & 0 \\ 0 & 0 & 0 \end{bmatrix}, \qquad \mathbf{a} = \begin{bmatrix} 1 \\ 0 \\ 0 \end{bmatrix}, \qquad \sigma^{\text{pind}} = \mathbf{0}$$

$$I_1 = 0\,, \qquad I_2 = 0\,, \qquad I_4 = y_a$$

$$\rightsquigarrow \qquad f = \alpha_4 I_4^2 - 1 = 0$$

$$\boxed{\alpha_4 := 1/y_a^2} \tag{22}$$

2. simple shear in the plane perpendicular to the fiber (transverse shear)

$$\sigma = \operatorname{dev}\sigma = \sigma^{\text{pind}} = \begin{bmatrix} 0 & y_{tr} & 0 \\ y_{tr} & 0 & 0 \\ 0 & 0 & 0 \end{bmatrix}, \qquad \mathbf{a} = \begin{bmatrix} 0 \\ 0 \\ 1 \end{bmatrix}$$

$$I_1 = y_{tr}^2\,, \qquad I_2 = 0\,, \qquad I_3 = 0\,, \qquad I_4 = 0$$

$$\rightsquigarrow \qquad f = \alpha_1 y_{tr}^2 - 1 = 0$$

$$\boxed{\alpha_1 := 1/y_{tr}^2} \tag{23}$$

3. simple shear in the fiber plane (in-plane shear)

$$\sigma = \operatorname{dev}\sigma = \sigma^{\text{pind}} = \begin{bmatrix} 0 & y_{ip} & 0 \\ y_{ip} & 0 & 0 \\ 0 & 0 & 0 \end{bmatrix}, \qquad \mathbf{a} = \begin{bmatrix} 1 \\ 0 \\ 0 \end{bmatrix}$$

$$I_1 = 0\,, \qquad I_2 = y_{ip}^2\,, \qquad I_3 = 0\,, \qquad I_4 = 0$$

$$\rightsquigarrow \qquad f = \alpha_2 y_{ip}^2 - 1 = 0$$

$$\boxed{\alpha_2 := 1/y_{ip}^2} \tag{24}$$

4. uniaxial tension and uniaxial compression perpendicular to the fiber

$$\sigma = \begin{bmatrix} 0 & 0 & 0 \\ 0 & 0 & 0 \\ 0 & 0 & y_{uni} \end{bmatrix}, \qquad \mathbf{a} = \begin{bmatrix} 1 \\ 0 \\ 0 \end{bmatrix}$$

$$I_1 = \frac{y_{uni}^2}{4}\,, \qquad I_2 = 0\,, \qquad I_3 = y_{uni}\,, \qquad I_4 = 0$$

$$\rightsquigarrow \qquad f = \alpha_1 \frac{y_{uni}^2}{4} + \alpha_3 y_{uni} + \alpha_{23} (y_{uni})^2 - 1 = 0$$

The parameter $\alpha_1$ is known from the second material test (transverse shear), thus two parameters $\alpha_3$ and $\alpha_{32}$ remain to be determined. Inserting in the yield function for $y_{uni}$, the yield stresses from uniaxial tension $y_{ut}$ and uniaxial compression $y_{uc}$ leads to a system of equations with two equations and two unknowns from which the parameters $\alpha_3$ and $\alpha_{32}$ can be obtained:

$$\boxed{\alpha_{32} := \frac{\dfrac{1}{y_{ut}} - \dfrac{1}{y_{uc}} - \dfrac{\alpha_1}{4}(y_{ut} - y_{uc})}{y_{ut} - y_{uc}}} \tag{25}$$

$$\boxed{\alpha_3 := \frac{1}{y_{ut}} - \frac{\alpha_1}{4} y_{ut} - \alpha_{32} y_{ut}} \tag{26}$$

### 2.4 Novel Invariant-based Quadratic Failure Criterion (IQC) and Softening Formulation

The developed stress-based failure criterion distinguishes between fiber failure (FF) and inter-fiber failure (IFF). The inter-fiber failure criterion takes interactions between normal and shear stresses as well as interactions between transverse and in-plane shear stresses into account. Further, different failure modes are regarded and a strain energy release rate formulation combined with the introduction of an internal length scale ensures mesh independent solutions in the softening regime.

#### 2.4.1 Fiber Failure Condition

It is assumed, that the strength in fiber direction is mainly governed by the strength of the fibers and that the fibers are only subject to stresses in fiber direction. Therefore, the fiber failure condition is rather simple:

$$\frac{\mathbf{a}\sigma\mathbf{a}}{R_{\parallel}} = 1 \tag{27}$$

The fiber tensile strength $R^t_{\parallel}$ and a compressive strength $R^c_{\parallel}$, representing the resistance of the UD-Composite under uniaxial tension and compression in fiber direction, are needed as input data. If one of these strengths is achieved, the material fails and there is no remaining load carrying capacity. The term $\mathbf{a}\sigma\mathbf{a}$ is the projection of the stress tensor onto the preferred direction and $R_{\parallel}$ is the resistance of the fiber bundle in fiber direction in tension ($R_{\parallel} = R^t_{\parallel}$) and in compression ($R_{\parallel} = R^c_{\parallel}$) respectively.

#### 2.4.2 Inter-Fiber Failure Condition

Inter-fiber failure is formulated in the format of the yield locus Eq. 18, based on the invariants presented there. The fourth invariant $I_4$ is omitted, because for loading in fiber direction the fiber failure criterion is activated, see Eq. 27. The failure surface is:

$$r = \beta_1 I_1 + \beta_2 I_2 + \beta_3 I_3 + \beta_{32} I_3^2 - 1 \tag{28}$$

The failure criterion is fulfilled, when $r = 0$. The parameters $\beta_1$, $\beta_3$ and $\beta_{32}$ are obtained in the same manner as the parameters $\alpha_1$, $\alpha_3$ and $\alpha_{32}$ for the yield function Eq. 18. Therefore, the material strengths of uniaxial tension $R^t_{\perp}$ and compression $R^c_{\perp}$ perpendicular to the fiber and the material strength of transverse shear $R_{\perp\perp}$ and in-plane shear $R_{\parallel\perp}$ have to be inserted instead of the yield stresses in Eq. 18. If not available from experimental tests, the required strengths $R^t_{\perp}$, $R^c_{\perp}$, $R_{\perp\perp}$ and $R_{\parallel\perp}$ can be obtained from micromechanical unit cell computations [Ernst, Vogler, Hühne,

and Rolfes (2010); Rolfes, Ernst, Vogler, and Hühne (2008)]. If the inter-fiber failure condition is achieved, the current stress state is saved as effective stress, i.e. all hardening moduli are set to zero and ideally plastic behavior is assumed. Stiffness degradation is then initiated and controlled by a scalar damage variable $d$. Here, the damage variable $d$ does not affect the stresses in fiber direction $\sigma_{11}$. Fig. 2 shows yield and fracture surface in the $\sqrt{I_1}$-$I_3$-invariant-plane, where $I_3$ accounts for biaxial and triaxial stress states and $\sqrt{I_1}$ stands for deviatoric stresses.

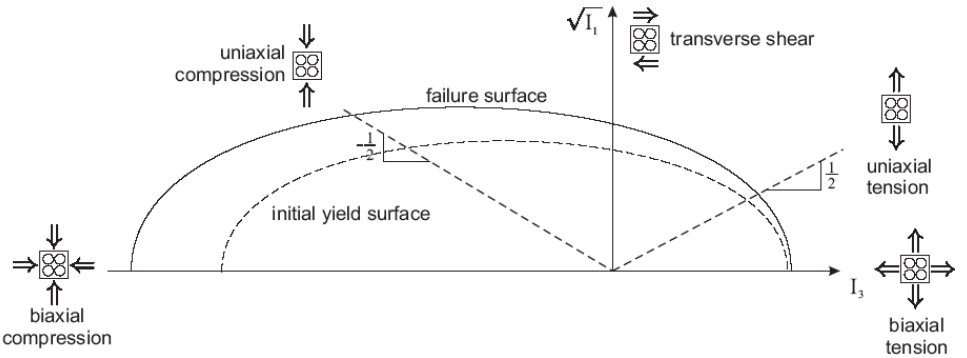


Figure 2: Yield and failure surface of the transversely-isotropic material model in $\sqrt{I_1}$-$I_3$-invariant-plane

### *2.4.3 Softening Formulation*

If the failure criterion is fulfilled, an exponential softening formulation is applied. Two different damage variables are used for FF and IFF. If the IQC detects IFF, the plasticity algorithm changes from plastic hardening to ideally plastic behavior, and an isotropic damage variable is multiplied with the effective plastic stress to give the nominal stresses. The evolution of the damage variable is governed by the fracture energy regularization technique, i.e. dependent on strain energy release rate and equivalent plastic displacement since damage initiation. All elastic constants, apart from the stiffness in fiber direction are damaged in the same way. Therefore, only fiber stresses remain in the element. If FF is detected, the fiber direction stresses are degraded with a formulation analogous to Hillerborg's softening [Hillerborg, Modeer, and Petersson (1976)]. The damage variable $d_f$ is calculated from the displacement at damage initiation

$$u_{fail}^{t,c} = L_e \frac{R_{\parallel}^{t,c}}{E_{\parallel}} \tag{29}$$

and the displacement at ultimate failure

$$u_{ult}^{t,c} = 2\frac{G_{Ic}}{R_{\|}^{t,c}} + u_{fail}^{t,c} \tag{30}$$

and the actual displacement $u$ with

$$d_f = \frac{u - u_{fail}}{u_{ult} - u_{fail}} \,. \tag{31}$$

The nominal stresses are then calculated by multiplication of the fiber direction stresses with the damage variable $d_f$.
The presented material model is implemented as a user subroutine into the user defined programming interface VUMAT for Abaqus Explicit and into the user defined programming interface UMAT for Abaqus Implicit. For an implicit analysis, the algorithmic consistent material tangent is required, which is obtained numerically. In order to assure numerical stability in the softening regime and to enforce the elastic plastic material tangent to remain positive definite , a visco-plastic regularisation is applied according to [Duvaut and Lions (1976)].

## 3 Results

Subsequently, three examples are chosen in order to demonstrate the applicability of the novel IQC failure criterion and the nonlinear material model developed. At first, different laminate lay-ups of the World Wide Failure Exercise (WWFE) [Hinton, Kaddour, and Soden (2004)] are modelled and experimentally obtained failure envelopes as well as the stress strain curves from uniaxial and biaxial tensile tests are compared to simulations. Secondly, a four-point-bending test of a curved composite beam consisting of 22 layers of a uniaxial carbon fiber reinforced composite is simulated. The 4-point bending test imposes a pure bending moment at the curved region of the beam and the stresses into thickness direction cause intra laminar failure leading to final collapse of the composite beam. In a third example, the initiation and propagation of cracks in an embedded 90°-layer is simulated by modelling the discontinuous material behavior at sub-ply level.

### *3.1 Laminate Models and Load Cases from the WWFE*

In the World Wide Failure Exercise, conceived and conducted by [Hinton, Kaddour, and Soden (2004)] a multitude of different laminate configurations and single UD-layers are investigated experimentally and compared to common used failure criteria. The laminate lay-ups, which are simulated with the novel material and failure model, are illustrated in Fig. 3. Further lay-ups are modelled and discussed

in [Ernst (2009)]. In order to get the $\sigma_1 - \sigma_2$-failure surface for each laminate experimentally, cylindrical test specimen are manufactured. These cylindrical tubes then are subjected to internal pressure superimposed by axial loading and torsion. Hence, the whole range of stress states from uniaxial loading over biaxial stress states to pure shear loading can be covered. For the detailed test setup and the exact material data the reader is referred to the WWFE [Hinton, Kaddour, and Soden (2004)]. The following table gives an assignment of laminate lay-ups and the chosen WWFE Load Cases:

- $(\pm 45°)_s$-laminate: E-glass fibers and epoxy resin MY750/HY917/DY063,
  WWFE Load Case 6 and WWFE Load Case 8
- $(0°/90°)_s$-laminate: E-glass fibers and epoxy resin MY750/HY917/DY063,
  WWFE Load Case 12
- $(0°/\pm 45°/90°)_s$-laminate: Carbon fibers AS4 and epoxy resin 3501-6.
  WWFE Load Case 14

In order to reproduce the real test situation in the finite element model, it is assumed that the load is applied on an infinite shell. Thus, no free-edge effects or inter-laminar shear stresses have to be considered. Each lamina is represented by one element and the elements are stacked in z-direction. The faces of the elements are restricted to remain parallel to their reference configuration, but can deform freely.

*WWFE Load Case 6: $\sigma_x$-$\sigma_y$-failure envelope of a $0°/\pm 45°/90°)_s$-laminate*

Failure envelopes of Puck [Puck and Schürmann (2004)] and IQC for FF in the $\sigma_y$-$\sigma_x$-plane compared with test data are shown in Fig. 4. In this load case the differences between Puck's criterion and IQC are negligible. Buckling in the tests might be an explanation of the overestimation of the compressive strengths of both models. Under mixed tension/compression the IQC reproduces the test results slightly better.

*Load Case 8: Biaxial $\sigma_y/\sigma_x = 2/1$-loading of a $0°/\pm 45°/90°)_s$-laminate*

In Fig. 5, computationally obtained stress-strain curves for a force-driven biaxial $\sigma_y/\sigma_x = 2/1$ tensile load using IQC are shown and compared with test data. A very good agreement of the simulation curves with the experimental data and the reported failure modes can be seen. The experimentally observed matrix cracking coincides perfectly with the inter-fiber failure (IFF) detected in the simulation.

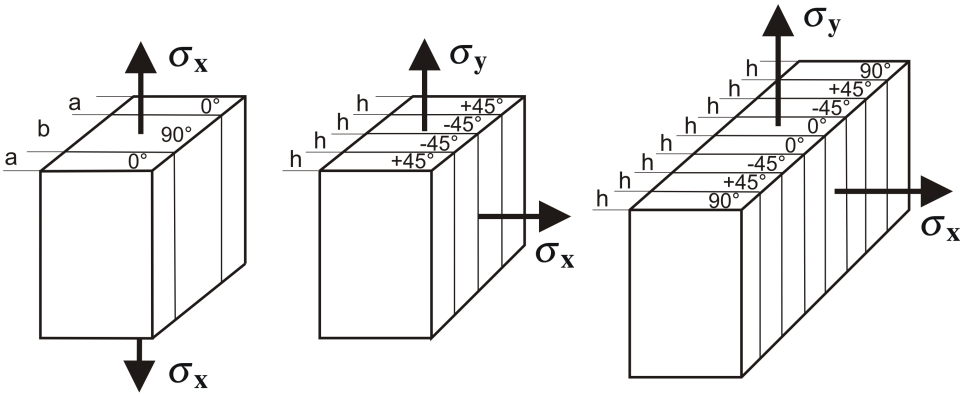


Figure 3: Laminates from the WWFE [Hinton, Kaddour, and Soden (2004)].
$(0°/90°)_s$, total thickness: 1.04 mm, b = 0.52 mm, a = 0.26 mm
$(\pm 45°)_s$, total thickness: 1.00 mm, h = 0.25 mm
$(0°/\pm 45°/90°)_s$, total thickness: 1.1 mm, h = 0.1375 mm

Considering the $\varepsilon_y$ branch in Fig. 5, the simulation with the IQC material model lies nearly exactly on the experimentally measured stress strain curve. Especially the nonlinearities after matrix cracking are very well predicted in the simulation. Considering the $\varepsilon_x$ branch, the nonlinearities are a little bit overestimated. Furthermore, the final failure of the laminate is predicted exactly by the IQC. The uppermost measuring points do not exactly coincide with the final failure (see Fig. 5), but they are rather the last gauge detection during the test, as stated by [Hinton, Kaddour, and Soden (2004)]. Final failure is reported at $857MPa$, which coincides accurately with the prediction of the IQC criterion.

*Load Case 12: Uniaxial $\varepsilon_y$-loading of a $(0°/90°)_s$-laminate*

Stress-strain curves for a $(0°/90°)_s$ laminate exposed to a displacement-driven tensile loading $\varepsilon_x : \varepsilon_y = 1 : 0$ are shown in Fig. 6. There is a very good correlation of the simulation with Puck's criterion and IQC compared with test data. Initial laminate damage due to tensile matrix failure in the 0°layer is predicted with IQC at approximately $90MPa$, whereas [Hinton, Kaddour, and Soden (2004)] report the onset of cracking at $117.5MPa$. There is no remarkable difference between the simulation with IQC and with Puck's criterion. Concerning final failure (FF), the IQC prediction is a little closer to the experimental data, but it also slightly overestimates the ultimate load.

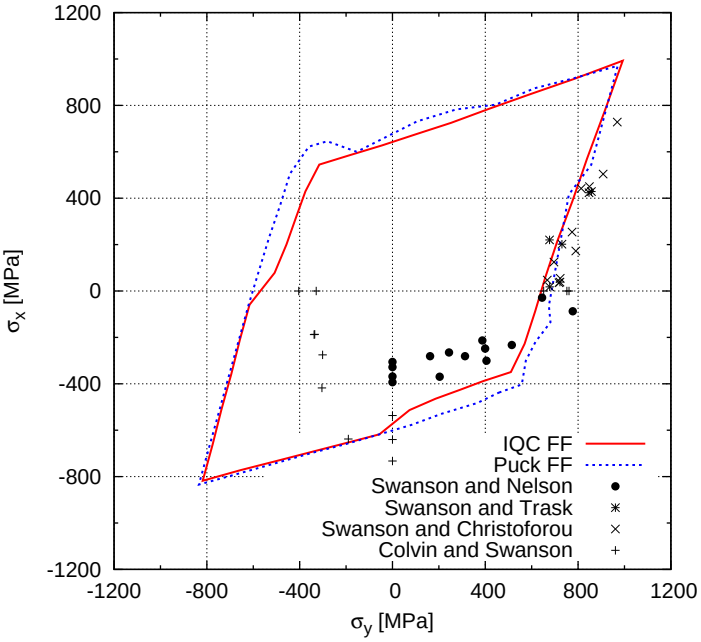


Figure 4: Load case 6: $\sigma_y$-$\sigma_x$-failure envelope for AS4/3501-6 $(0°/\pm45°/90°)_s$-Laminate - Test data and prediction with Puck and IQC

*Load Case 14:* $\sigma_y/\sigma_x = 1/-1$ *of a* $(\pm45°)_s$*-Laminate*

In Fig. 7, stress-strain curves obtained by simulation with Puck failure criterion and IQC criterion for a force-driven biaxial $\sigma_y/\sigma_x = 1/-1$ load are depicted and compared with test data. The experimentally observed nonlinear behavior prior to failure is characteristic for this load case. The IQC criterion is used with the nonlinear material model presented as well as with a linear elastic material model. All three simulations (Puck linear, IQC linear and IQC nonlinear) predict the inter-fiber failure at $\sigma_y \cong 70$ MPa and are thus in exact agreement with the test data. But, considering the nonlinear material behavior, it is obvious, that Puck as well as IQC in conjunction with a linear elastic material law are not able to reproduce the experimentally observed behavior at all. The failure strains are considerably underestimated, see Fig. 7. The IQC failure criterion used with the nonlinear elastic plastic material law presented in Sec. 2 is able to recover the nonlinear material behavior in numerical simulation. Considering loading in $x$-direction, the experimentally determined inter-fiber failure is exactly predicted by the IQC nonlinear at 3.8% (compare right-hand side in Fig. 7) and the failure strain for inter-fiber failure

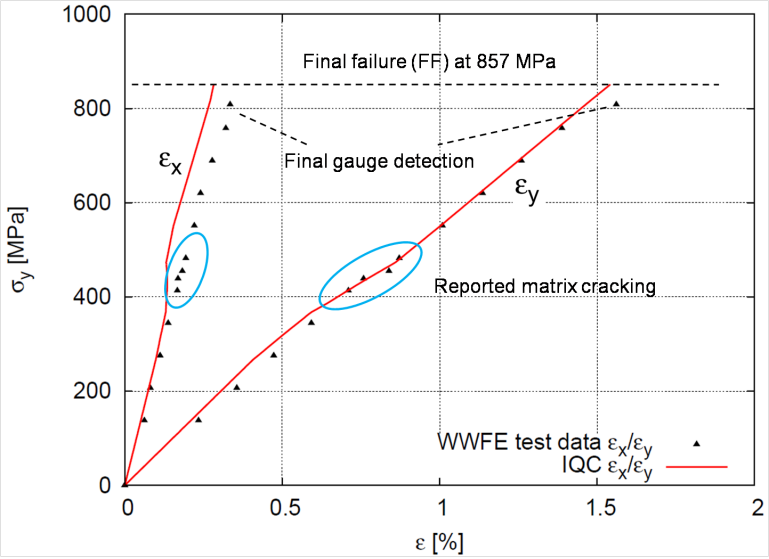


Figure 5: Load case 8: stress strain curves for AS4/3501-6 $(0°/\pm45°/90°)_s$-Laminate under biaxial tensile loading with $\sigma_y/\sigma_x = 2/1$

in $y$-direction is slightly overestimated. This example demonstrates the necessity for regarding the pre-failure nonlinearities illustrated in Fig. 1 in order to improve the modelling approaches for fiber reinforced polymers.

### *3.2 Curved composite beam*

In order to determine the delamination resistance of a layered composite beam, a serial of 4-point bending tests was conducted at Airbus Germany [Airbus (2006)]. The experimental setup is depicted in Fig. 8. Out of plane normal tensile stresses are crucial for the onset of delamination. Therefore, the test specimen is exposed to a pure bending moment in a well defined area in order to determine the out-of-plane normal allowable tension. The test specimen consist of 22 UD-layers. Each layer has a thickness of $t = 0.25mm$, the thickness of the specimen is $t = 5.5mm$. A sketch of the spar sample is depicted in Fig. 9. The FE model is discretized in the commercial finite element code Abaqus. Linear 8-node continuum elements (C3D8) are used to model the beam. The bending moment is applied on rigid plates which are tied to the two ends of the beam. Displacement boundary conditions are set to prevent rigid body translations and rotations of the whole system. The number of elements in thickness direction is set to 30, with 60 elements in circumferential direction of the curved segment and 10 elements in width. Only

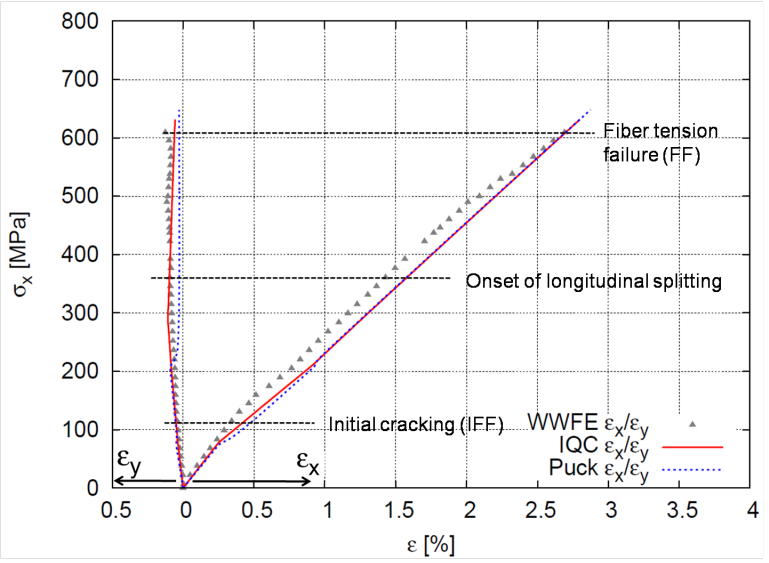


Figure 6: Load case 12: stress-strain curves for E-glass/MY750/HY917/DY063 $(0°/90°)_s$-Laminate under uniaxial tensile loading with $\sigma_x : \sigma_y = 1 : 0$

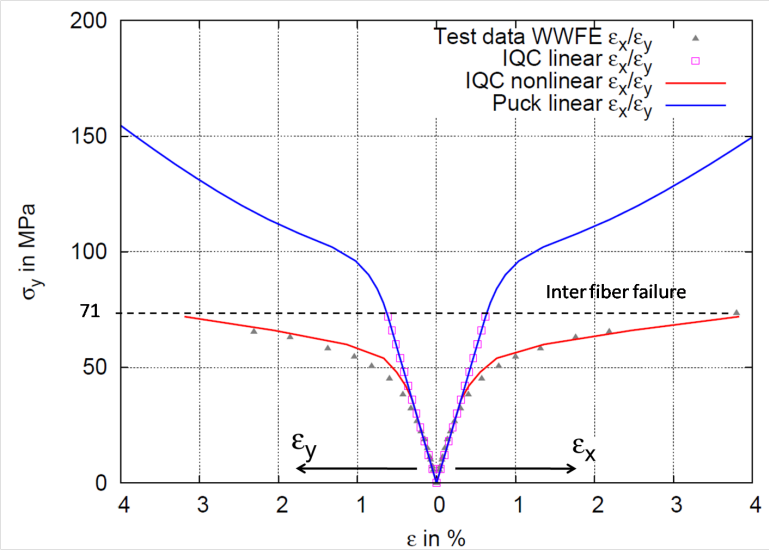


Figure 7: Load case 14: stress-strain curves for E-glass/MY750/HY917/DY063 $(\pm 45°)_s$-Laminate under biaxial tensile loading with $\sigma_y : \sigma_x = 1 : -1$

the curved region of the beam is modelled with the IQC material model, the legs of the composite beam are modelled with an transversely-isotropic elasticity law without damage. The reason therefore is, that in the region of load application very high pressures occur, which causes premature failure in the contact layers. In Fig. 9 on the right hand side an FE model of the curved composite beam is depicted. Fig. 11 shows the simulated overall load-displacement curve compared to experimental test data. Interestingly, edge delaminations occur just before delamination in the middle layer starts, as marked in Fig. 11. Supposably, these edge delaminations can be traced back to the the edge effect, e.g transverse shear stresses cause peeling stresses which induce delamination at the edge of the laminate. Whether these edge delaminations are observed in the experiments is not documented in the technical report [Airbus (2006)]. The left hand side of Fig. 10 shows edge delaminations and delaminations in a medial layer shortly before final collapsing of the beam. Fig. 10 on the left hand side shows the damage variable $d$, plotted in a vertical cut through the beam. It can be seen, that delaminations occur shortly below the middle plane of the test specimen which is in a good agreement with the experiments, compare Fig. 8 on the left. These delaminations finally yield to a separation of the composite beam. They are caused by out of plane normal tensile stresses and in-plane shear stresses, but mainly the out of plane stresses contribute to delaminations. Considering the overall load displacement curves, depicted in Fig. 11, the simulations tend to be slightly stiffer than the experimentally obtained curves, whereas the ultimate load is predicted quite well. The oscillations in the simulated load-displacement-curve are due to the contact formulation used in the model. In summary, it can be stated, that the overall load displacement behavior as well as the different failure mechanisms are predicted very well.

### *3.3 Simulation of the in-situ effect*

As a further example, the in-situ effect is investigated, showing the degradation of stiffness due to the characteristic damage state in the mid layer of a $(0°90°)_s$ laminate. It is shown, that the experimentally observed stiffness degradation of an inside 90° layer can be recovered in numerical simulation by modelling the actual discontinuous material behavior of the embedded laminae on sub-ply level. For reasons of computational efficiency one eighth of the original test specimen is modelled exploiting symmetry. Eight-node solid elements (Abaqus C3D8 elements) are used in the fully three-dimensional model. In order to capture the in-situ effect on sub-ply level, a discretization of at least 4 elements over the thickness of the embedded layer proved to be necessary. Fig. 13 shows the saturated crack density in the intermediate layer. At first, several cracks evolve caused be inter-fiber failure in the 90° layer. In Fig. 13 on the right a cut between the 0°-layer and the 90°-layer

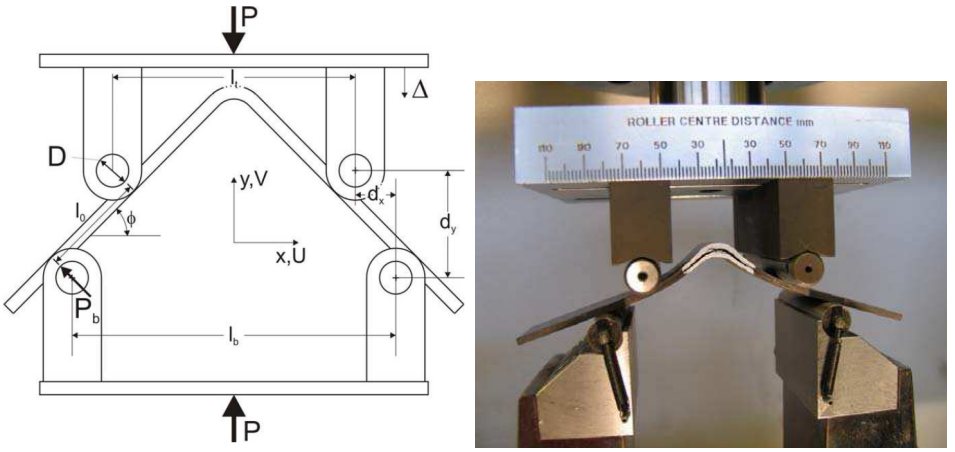


(a) Experimental setup (b) Post failure state

Figure 8: Experimental setup of 4-point bending test of a curved composite beam

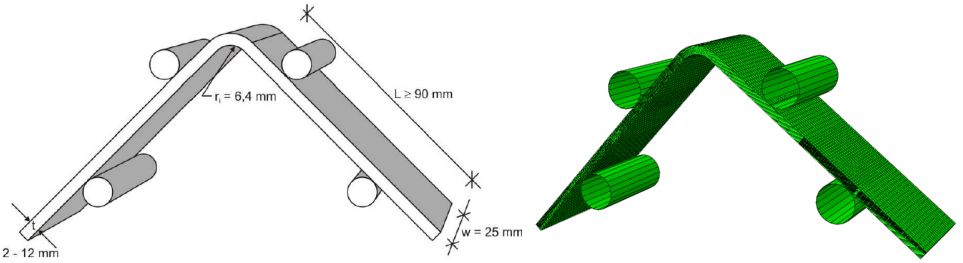


(a) Test specimen geometry (b) FE model

Figure 9: 4-point bending test, geometry and fe-model

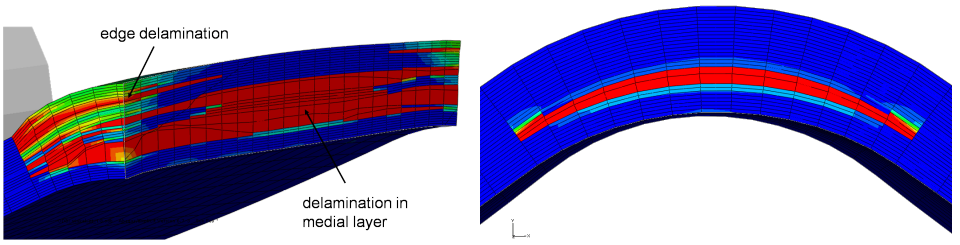


(a) Transverse cut (b) Longitudinal cut

Figure 10: Delamination in curved composite beam: plot of damage variable $d$

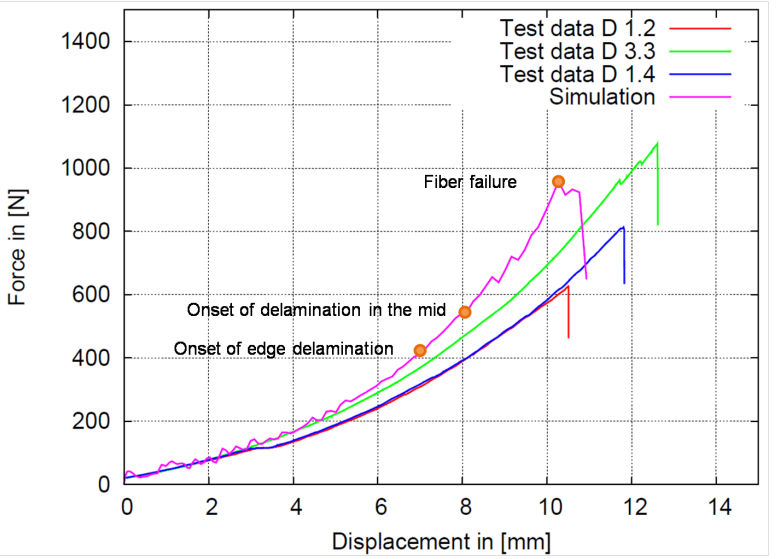


Figure 11: Load-displacement curves: Test results and simulation

is depicted, showing a plot of the scalar damage variable $d$. It can be seen, that delamination is initiated by inter-fiber failure cracks in the 90°-layer. In the red colored region, the damage variable has reached the value 1, i.e. delamination has occurred. In Fig. 14 the homogenized stress-strain relation of the whole laminate is depicted and compared to the stress-strain relation of the 0° outside layers only. Thus, the contribution of the intermediate layer to the overall load carrying capacity can be evaluated. It should be noted, that this homogenized stress strain relation is the result of simulating the actual discontinuous material of a ply embedded in a laminate with the developed transversely-isotropic continuum damage approach. Both the propagation of cracks due to inter-fiber failure and the saturated damage state in the mid layer are recovered in the numerical simulations. As depicted in Fig. 14 the onset of crack propagation starts at a strain level of 0.17 in the mid layer. Than, a reduction of stiffness can be observed until the characteristic damage state is achieved at a strain level of 0.22. In Fig. 15, experimentally obtained and simulated degradation factors $\eta_E$ for the elastic modulus of the embedded 90° layer are plotted. Experimental data are taken from [Knops (2003)].

## 4 Conclusion

In the presented work, a sub-ply level continuum damage mechanics model for fiber reinforced polymer laminates is proposed, covering shear nonlinearities, a novel in-

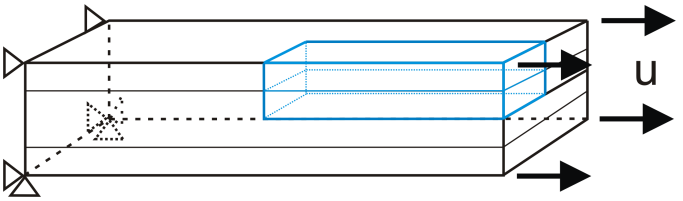


Figure 12: $(0°90°)_s$ laminate: boundary conditions and loading

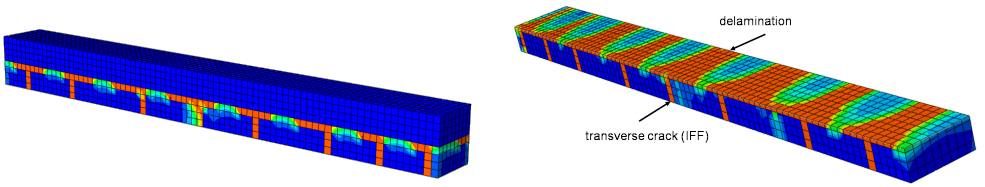


(a) Characteristic damage state

(b) Cut between 0°90°-layer: Onset of delamination, caused by inter-fiber failure

Figure 13: Characteristic damage state: Damage variable $d$

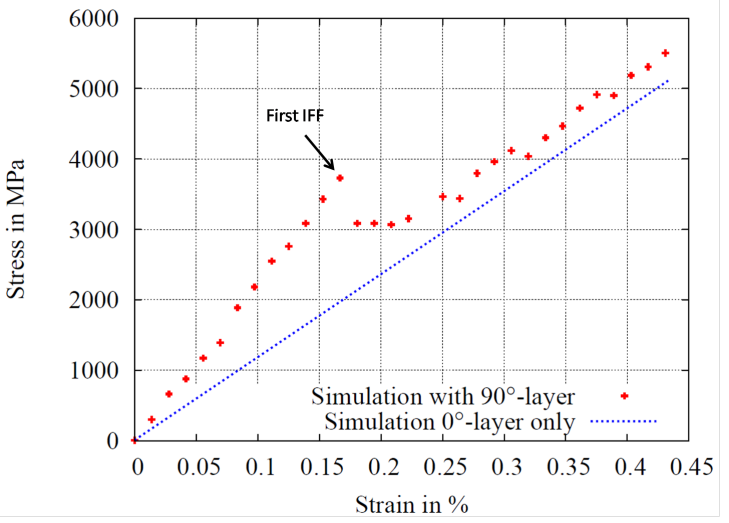


Figure 14: Stiffness degradation of the laminate, caused by inter-fiber failure

variant based quadratic criterion for the onset of failure and a softening formulation regarding different fracture energies in dependence of the failure mode. The applicability of the novel material and failure model is shown on three examples. At first,

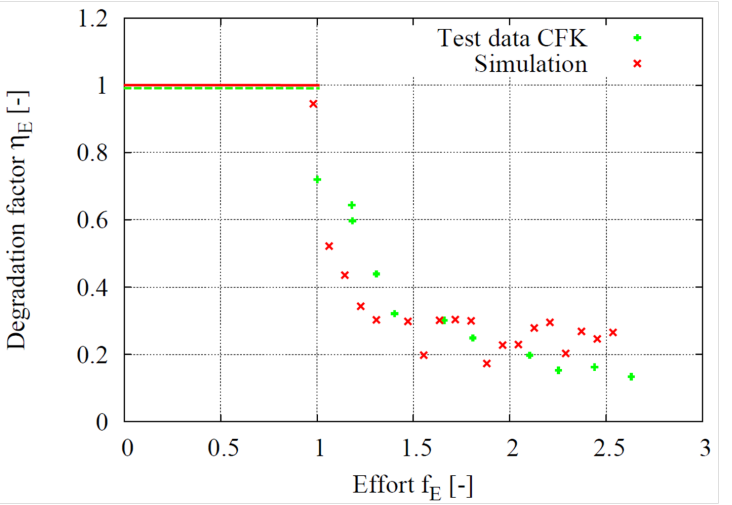


Figure 15: Degradation factor $\eta_E$ versus effort $f_E$ for E-modulus of the embedded 90° layer, simulation and test data [Knops (2003)]

different laminate configurations are simulated and compared to test data from the WWFE. Both, the failure surface and the stress-displacement behavior under uniaxial and biaxial loading are predicted. Furthermore, it is shown, that not only the onset of failure, but also nonlinearities especially under shear are to be considered in order to obtain a realistic experimentally observed stress-strain behavior. This is shown on the WWFE load case 14. Secondly, a four point bending test of a curved composite beam is simulated and compared to test data. The overall load displacement behavior can be predicted as well as the delamination, caused by inter-fiber failure. In a third example, the stiffness reduction of embedded 0° layer due to inter-fiber failure can be simulated by modelling the actual discontinuous material behavior on sub-ply level.

**Acknowledgement:** Part of this work was funded by the German Research Council (DFG). This support within the framework of SPP-1123 "Textile composite design and manufacturing technologies for lightweight structures in mechanical and vehicle engineering" is gratefully acknowledged. Furthermore, the authors would like to express their sincere thanks to Dr. Guido Kuhlmann and Airbus Deutschland for providing experimental data of the curved composite beam.

## References

**Airbus** (2006): Test results of L-angle 4-point bending tests. Technical report, ESWNG, Testing Technology Germany, Hamburg, 2006.

**Allix, O.; Corigliano, A.** (1999): Geometrical and interfacial non-linearities in the analysis of delamination in composites. *International Journal of Solids and Structures*, vol. 36, no. 15, pp. 2189 – 2216.

**Allix, O.; Feissel, P.; Thévenet, P.** (2003): A delay damage mesomodel of laminates under dynamic loading: basic aspects and identification issues. *Computers & Structures*, vol. 81, no. 12, pp. 1177 – 1191.

**Barbero, E. J.; Cortes, D. H.** (2010): A mechanistic model for transverse damage initiation, evolution, and stiffness reduction in laminated composites. *Composites Part B: Engineering*, vol. 41, no. 2, pp. 124 – 132.

**Boehler, J.**(Ed): *Applications of Tensor Functions in Solid Mechanics*. CISM No. 292. Springer.

**Camanho, P.; Dávila, C.; Moura, M.** (2003): Numerical simulation of mixed-mode progressive delamination in composite materials. *Journal of Composite Materials*, vol. 37, no. 16, pp. 1415 – 1438.

**Cuntze, R.; Freund, A.** (2004): The predictive capability of failure mode concept-based strength criteria for multidirectional laminates. In Hinton, M.; Kaddour, A.; Soden, P.(Eds): *Failure criteria in fibre reinforced polymer composites: The World-Wide Failure Exercise*, pp. 429–489. Elsevier Science, Oxford.

**Duvaut, G.; Lions, J.** (1976): *Inequalities in Mechanics and Physics*. Springer Verlag, Berlin.

**Eidel, B.** (2004): *Anisotropic Inelasticity - Modelling, Simulation, Validation*. PhD thesis, Fachbereich Bauingenieurwesen und Geodäsie, Technische Universität Darmstadt, 2004.

**Ernst, G.** (2009): *Multiscale Analysis of Textile Composites -Stiffness and Strength-*. PhD thesis, Leibniz Universität Hannover, 2009. Mitteilungen des Instituts für Statik und Dynamik der Leibniz Universität Hannover 10/2009.

**Ernst, G.; Vogler, M.; Hühne, C.; Rolfes, R.** (2010): Multiscale progressive failure analysis of textile composites. *Composites Science and Technology*, vol. 70, no. 1, pp. 61 – 72.

**Hallett, S.; Green, B.; Jiang, W.; Wisnom, M.** (2009): An experimental and numerical investigation into the damage mechanisms in notched composites. *Composites Part A: Applied Science and Manufacturing*, vol. 40, no. 5, pp. 613 – 624.

**Hashin, Z.** (1980): Failure Criteria for Unidirectional Fiber Composites. *Journal of Applied Mechanics*, vol. 47, pp. 329–334.

**Hillerborg, A.; Modeer, M.; Petersson, P. E.** (1976): Analysis of crack formation and crack growth in concrete by means of fracture mechanics and finite elements. *Cement and Concrete Research*, vol. 6, pp. 773–782.

**Hinton, M. J.; Kaddour, A. S.; Soden, P. D.** (2004): *Failure Criteria in Fibre Reinforced Polymer Composites: The World-Wide Failure Exercise*. Elsevier Science, Oxford.

**Knops, M.** (2003): *Sukzessives Bruchgeschehen in Faserverbundlaminaten*. PhD thesis, Fakultät für Maschinenwesen der Rheinisch-Westfälischen Technischen Hochschule Aachen, 2003.

**Krueger, R.; Paris, I. L.; O'Brien, T. K.; Minguet, P. J.** (2002): Comparison of 2d finite element modeling assumptions with results from 3d analysis for composite skin-stiffener debonding. *Composite Structures*, vol. 57, no. 1-4, pp. 161 – 168.

**Ladevèze, P.; Allix, O.; Deü, J.-F.; Lèvêque, D.** (2000): A mesomodel for localisation and damage computation in laminates. *Computer Methods in Applied Mechanics and Engineering*, vol. 183, no. 1-2, pp. 105 – 122.

**Maimí, P.; Camanho, P.; Mayugo, J.; Dávila, C.** (2007): A continuum damage model for composite laminates: Part i - constitutive model. *Mechanics of Materials*, vol. 39, no. 10, pp. 897 – 908.

**Maimí, P.; Camanho, P.; Mayugo, J.; Dávila, C.** (2007): A continuum damage model for composite laminates: Part ii - computational implementation and validation. *Mechanics of Materials*, vol. 39, no. 10, pp. 909 – 919.

**Maimí, P.; Mayugo, J. A.; Camanho, P. P.** (2008): A three-dimensional damage model for transversely isotropic composite laminates. *Composite Materials*, vol. 42, no. 25/2008.

**Nahas, M. N.** (1986): Survey of Failure and Post-Failure Theories of Laminated Fiber-Reinforced Composites. *Composites Technology & Research*, vol. 8, no. 4, pp. 138–153.

**Pinho, S.; Dávila, C.; Ianucci, L.; Robinson, P.** (2004): Failure models and criteria for frp under in-plane or three-dimensional stress states including shear non-linearity. *NASA/TM-2003-213530*.

**Puck, A.** (1996): *Festigkeitsanalyse von Faser-Matrix-Laminaten, Modelle für die Praxis*. Hanser, München.

**Puck, A.; Schneider, W.** (1969): On failure mechanisms and failure criteria of filament-wound glass-fibre/resin composites. *Plastics and Polymers*, vol. 37, pp. 33–44.

**Puck, A.; Schürmann, H.** (2004): Failure analysis of FRP laminates by means of physically based phenomenological models. In Hinton, M. J.; Kaddour, A. S.; Soden, P. D.(Eds): *Failure Criteria in Fibre Reinforced Polymer Composites: The World-Wide Failure Exercise*, pp. 264–297. Elsevier Science, Oxford.

**Rogers, T.** (1987): Yield criteria, flow rules and hardening in anisotropic plasticity. In Boehler, J.(Ed): *Yielding, damage and failure of anisotropic solids*, volume 5, pp. 53–79. EGF Publication.

**Rolfes, R.; Ernst, G.; Vogler, M.; Hühne, C.** (2008): Material and failure models for textile composites. In Camanho, P. P.; Dávila, C. G.; Pinho, S. T.; Remmers, J.(Eds): *Mechanical Response of Composites*, volume 10 of *Computational Methods in Applied Sciences*, pg. in print. Springer. ISBN: 978-1-4020-8583-3.

**Schröder, J.** (1995): *Theoretische und algorithmische Konzepte zur phänomenologischen Beschreibung anisotropen Materialverhaltens*. PhD thesis, Universität Hannover, 1995.

**Schuecker, C.; Pettermann, H.** (2006): A continuum damage model for fiber reinforced laminates based on ply failure mechanisms. *Composite Structures*, vol. 76, no. 1-2, pp. 162 – 173. Fifteenth International Conference on Composite Materials - ICCM-15.

**Spencer, A.** (1987): Kinematic constraints, constitutive equations and failure rules for anisotropic materials. In Boehler, J.(Ed): *Applications of Tensor Functions in Solid Mechanics*, CISM No. 292, pp. 187–201. Springer.

**Tsai, S. W.; Wu, E. M.** (1971): A general theory of strength for anisotropic materials. *Journal of Composite Materials*, vol. 5, pp. 58–80.

**Turon, A.; Camanho, P.; Costa, J.; Dávila, C.** (2006): A damage model for the simulation of delamination in advanced composites under variable-mode loading. *Mechanics of Materials*, vol. 38, no. 11, pp. 1072 – 1089.

**Turon, A.; Camanho, P.; Costa, J.; Renart, J.** (2010): Accurate simulation of delamination growth under mixed-mode loading using cohesive elements: Definition of interlaminar strengths and elastic stiffness. *Composite Structures*, vol. 92, no. 8, pp. 1857 – 1864.